CHEMISTRY OF MATERIALS

pubs.acs.org/cm Article

Quantifying Environmental Effects on the Solution and Solid-State Stability of a Phenothiazine Radical Cation

Aman Preet Kaur, Oliver C. Harris, N. Harsha Attanayake, Zhiming Liang, Sean R. Parkin, Maureen H. Tang,* and Susan A. Odom*

Cite This: *Chem. Mater.* 2020, 32, 3007−3017 Read Online

ACCESS | Metrics & More | Article Recommendations | Supporting Information

ABSTRACT: Organic radical cations are important intermediates in a wide variety of chemical processes. To date, significant progress has been made to improve the stability of these charged materials for use in electrochemical energy storage applications, especially in redox flow batteries. Here, we report the synthesis and isolation of four radical cation salts of *N*-(2-(2-methoxyethoxy)-ethyl)phenothiazine (MEEPT), synthesizing MEEPT-X where X is tetrafluoroborate (BF_4^-), hexafluorophosphate (PF_6^-), perchlorate (ClO_4^-), and bis(trifluoromethanesulfonyl)imide ($TFSI^-$), and a comparison of their stability in solution and in the solid state. In the solution, UV−vis spectroscopy and rotating ring-disk electrode voltammetry show similar stability trends with respect to anion identity, with the $TFSI^-$ salt being the most stable. In the solid state, these compounds show remarkable stability in air and at elevated temperatures, with the ClO_4^- salt surviving after being heated at 90 °C overnight in air. The different trends in MEEPT-X stability with X highlight the importance of concentration and the environment on the overall stability.

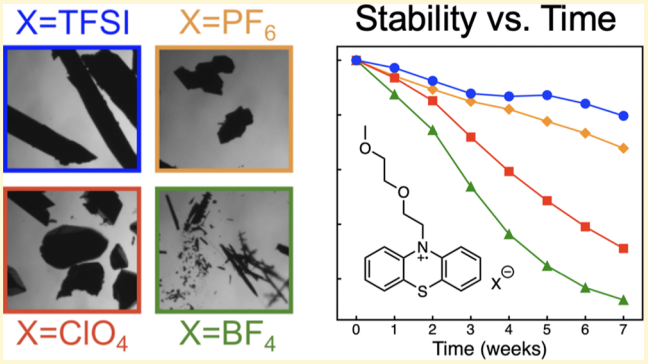

INTRODUCTION

Organic electroactive materials that exhibit stability over multiple oxidation states are of interest for a variety of charge transport and charge storage applications.[1−3] A number of redox chemistries based on organic electroactive materials have been proposed and investigated for redox flow batteries (RFBs), as they could serve as a much needed replacement of vanadium species—a material with limited abundance compared to the amount needed for large-scale storage and one that is subject to significant price fluctuations.[4−19] For these chemistries to be viable, one important requirement is that electron-donating (positive electrolyte) and -accepting (negative electrolyte) molecules need to be sufficiently stable across all states of charge accessed in an electrochemical cell. In nonaqueous RFBs, the charged species generated during battery cycling are almost always more reactive than their uncharged species and are prone to many degradation pathways.[6,20−23] Despite this, a variety of stable charged species have been identified and isolated. Among the active materials used on the positive side of RFBs, phenothiazine derivatives have been investigated as stable electron donors, with numerous radical cation salts having been isolated.[11,19,24,25] Additional organic positive active materials with stable charged forms in nonaqueous conditions include derivatives of nitroxides,[8] dimethoxybenzene,[26] phenazine,[15] and cyclopropenium.[16] Stable organic radical cations have also been widely used in synthetic chemistry. Their reactions have been investigated as oxidizing catalysts or initiators, and they mediate a significant number of transformations to construct C−C and C−X bonds.[27,28]

Applications that involve their use as energy-storing materials require the charged states to be stable in solution for a long period of time. However, identification of such species and assessment of their stability at concentrations of interest have proved to be quite challenging. There are reports in which the charged active electrolytes are only stable over an order of hours; these short-lived charged species are not suitable for the purposes of constructing a battery.[29] Some charged active electrolytes have been shown to not irreversibly decompose, but rather convert back to neutral (self-discharge); while the material is still useable, the coulombic efficiency of the battery suffers.[19,21] We are interested in studying charged organic compounds and predicting and understanding solution-state stability for applications with variable concentrations so that we can design stable materials for RFBs.

Received: December 24, 2019
Revised: February 21, 2020
Published: February 21, 2020

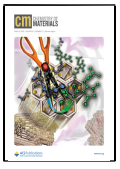

https://dx.doi.org/10.1021/acs.chemmater.9b05345
Chem. Mater. 2020, 32, 3007−3017

Further, we are interested in stability in the solid state. Before this study, we were not sure whether the species needed to be stored in a glovebox, for example, or be protected from light.

A variety of methods can be used to generate radical cation salts. These include chemical oxidation, electrochemical oxidation, radiolytic generation, and photoinduced electron transfer.[30,31] After generation, radical cations can be detected and analyzed by mass spectrometry, ultraviolet photoelectron spectroscopy, optical spectroscopy, and electron spin resonance (ESR).[30] With numerous methods being available for charged species generation, we are interested in comparing the reliability of the analysis of charged species generated by different methods and determining their effect on the stability of radical cations. Among these techniques, optical spectroscopy and ESR have been extensively used to study organic radical cations in solution.[23,32] Electrochemical generation by bulk electrolysis can be used to determine the stability at intermediate (10−50 mM) concentrations, whereas higher concentrations of species have been studied in cycling flow cells.

We previously studied *N*-(2-(2-methoxyethoxy)ethyl)-phenothiazine (MEEPT) and its tetrafluoroborate radical cation salt in flow cell cycling experiments, and found that the redox couple demonstrated excellent cell efficiency and stable cycling.[11] In addition to our ongoing efforts to modify the parent structure of MEEPT to investigate the effect of molecular structure on the stability of the charged state, we wanted to study the effect of the chemical environment to extend its application as an energy-storing material. To this end, we studied the effect of a series of counteranions (X^-) on MEEPT stability in solution and in the solid state. Here, we report the synthesis and characterization of radical cation salts with tetrafluoroborate (BF_4^-), hexafluorophosphate (PF_6^-), perchlorate (ClO_4^-), and bis(trifluoromethanesulfonyl)imide ($TFSI^-$) anions (Scheme 1). In addition to studying solid samples, we report on an analysis of stability in the solution state, which we evaluated using UV−vis spectroscopy and rotating ring-disk electrode voltammetry (RRDE). We also compared trends in solution to results of the shelf life (benchtop) and thermal stability in the solid state under variable conditions (e.g., varied atmospheres and temperatures) to evaluate the conditions in which these species remain stable.

Scheme 1. Synthesis of the Radical Cation Salts of *N*-(2-(2-Methoxyethoxy)ethyl)phenothiazine with Tetrafluoroborate (MEEPT-BF_4), Hexafluorophosphate (MEEPT-PF_6), Perchlorate (MEEPT-ClO_4), and Bis(trifluoromethanesulfonyl)imide (MEEPT-TFSI) as counterions

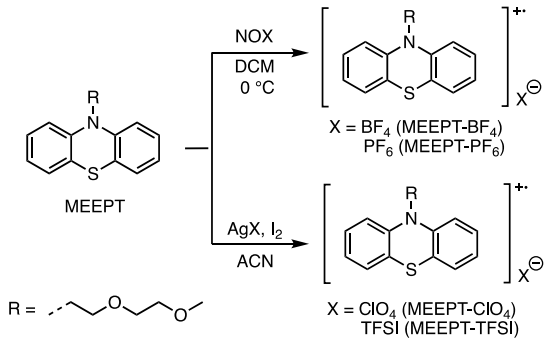

EXPERIMENTAL SECTION

Materials. *N*-[2-(2-Methoxyethoxy)ethyl]phenothiazine (MEEPT, CAS RN 2098786-35-5, >98%) was purchased from TCI America. Silver bis(trifluoromethanesulfonyl) imide (AgTFSI, > 98%) and silver perchlorate hydrate ($AgClO_4 \cdot xH_2O$, 99%) were purchased from TCI America and Sigma-Aldrich, respectively, and stored inside a refrigerator set at 4 °C. Nitrosonium tertrafluoroborate ($NOBF_4$, 98%) and hexafluorophosphate ($NOPF_6$, 96%) were purchased from Alfa Aesar and were stored and weighed in an argon atmosphere glovebox, and removed in a capped vial only immediately prior to use. Dichloromethane (DCM, 99.9%) and acetonitrile (ACN, 99.9%) for radical cation synthesis were purchased from Avantor (VWR) and were used from a solvent dispensing system (LC Technology Inc). Diethyl ether (ACS reagent grade) was obtained from Avantor (VWR).

Synthesis of Radical Cation Salts. *N-(2-(2-Methoxyethoxy)-ethyl)phenothiazinium Tetrafluoroborate (MEEPT-BF_4).* MEEPT (3.84 g, 12.7 mmol) was added to an oven-dried and cooled (to RT with a stream of nitrogen) 250 mL round-bottomed flask containing a stir bar. Anhydrous DCM (50 mL) was dispensed from a solvent-dispensing system into the flask and the resulting pale yellow solution was stirred under nitrogen for the subsequent steps. The reaction flask was then placed in an ice bath. $NOBF_4$ (1.56 g, 13.4 mmol) was added to the solution, which immediately turned dark orange. The reaction vessel was capped with a rubber septum and the reaction mixture was stirred for 1 h, after which diethyl ether (100 mL) was added gradually with continued stirring, producing a dark precipitate. The precipitate was filtered, then dissolved in DCM (50 mL) and re-precipitated with a second addition of diethyl ether (100 mL). This process was repeated once more to ensure removal of any unreacted starting material. The final precipitate was dried under vacuum to yield MEEPT-BF_4 as a dark brown solid (2.80 g, 57%). The product was then crystallized by dissolving it in DCM in small scintillation vials, which were placed inside a glass jar containing diethyl ether. The jar was capped and was placed in a freezer, and crystals (black needles, 76%) formed through vapor diffusion. The crystals were filtered and dried under vacuum. Anal. Calcd for $C_{17}H_{19}BF_4NO_2S$: C, 52.60; H, 4.93; N, 3.61. Found: C, 52.84; H, 4.98; N, 3.64.

N-(2-(2-Methoxyethoxy)ethyl)phenothiazinium Hexafluorophosphate (MEEPT-PF_6). MEEPT (5.00 g, 16.6 mmol) was added to an oven-dried and cooled (to RT with a stream of nitrogen) 250 mL round-bottomed flask with a stir bar. Anhydrous DCM (50 mL) was dispensed from a solvent-dispensing system into the flask and the resulting pale yellow solution was stirred under nitrogen for the subsequent steps. The reaction flask was then placed in an ice bath. $NOPF_6$ (3.20 g, 18.3 mmol) was added to the solution, which immediately turned dark orange. The reaction vessel was capped with a rubber septum and the reaction mixture was stirred under nitrogen for 1 h, after which diethyl ether (100 mL) was added gradually with continued stirring, producing a dark precipitate. The precipitate was filtered, then dissolved in DCM (50 mL), and re-precipitated with a second addition of diethyl ether (100 mL). This process was repeated once more to ensure removal of any unreacted starting material. The final precipitate was dried under vacuum to yield MEEPT-PF_6 as a dark brown solid (6.00 g, 81%). The product was then crystallized by dissolving it in DCM in small scintillation vials, which were placed inside a glass jar containing diethyl ether. The jar was capped and was placed in a freezer, and crystals (black blocks, 72%) formed through vapor diffusion. The crystals were filtered and dried under vacuum. Anal. Calcd for $C_{17}H_{19}F_6NO_2SP$: C, 45.74; H, 4.29; N, 3.14. Found: C, 45.79; H, 4.43; N, 3.14.

N-(2-(2-Methoxyethoxy)ethyl)phenothiazinium Perchlorate (MEEPT-ClO_4). MEEPT (2.00 g, 6.63 mmol) was added to an oven-dried and cooled (to RT with a stream of nitrogen) 100 mL round-bottomed flask with a stir bar. Anhydrous ACN (20 mL) was dispensed from a solvent-dispensing system and the resulting pale yellow solution was stirred under nitrogen for the subsequent steps. Then, iodine (0.842 g, 3.32 mmol) was added to the resulting solution after which a solution of $AgClO_4 \cdot xH_2O$ (1.44 g, 6.95 mmol)

https://dx.doi.org/10.1021/acs.chemmater.9b05345
Chem. Mater. 2020, 32, 3007−3017

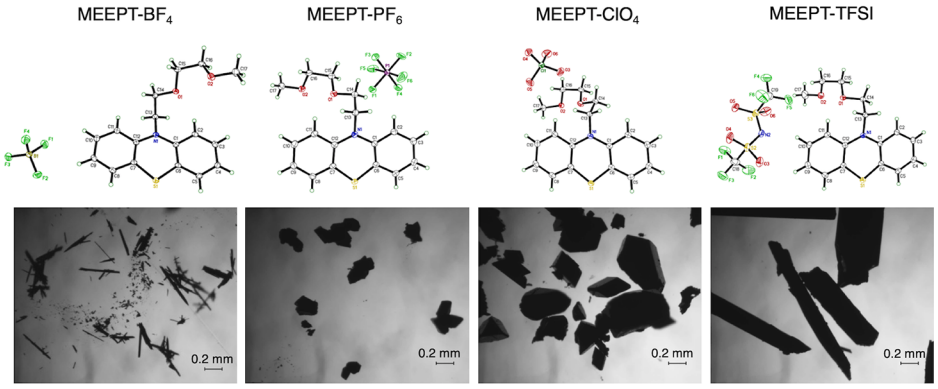

Figure 1. Thermal ellipsoid plots of the crystal structures (top) and microscope images of crystals (bottom) of *N*-(2-(2-methoxyethoxy)ethyl)-phenothiazinium radical cation salts (MEEPT-X) with X = tetrafluoroborate (BF_4^-), hexafluorophosphate (PF_6^-), perchlorate (ClO_4^-), or bis(trifluoromethanesulfonyl)imide ($TFSI^-$) as counterions.

in anhydrous ACN (10 mL) was added to the flask containing MEEPT and iodine. The reaction mixture turned dark orange and was stirred for 15 min, after which it was passed through a plug of Celite. The filtrate was concentrated to approximately 5 mL of ACN, after which diethyl ether (20 mL) was added, producing a dark precipitate. The resulting solid was washed with diethyl ether (20 mL) and hexanes (20 mL). The final precipitate was dried under vacuum to yield MEEPT-ClO_4 as a black crystalline solid (2.30 g, 86%). The product was then crystallized by dissolving it in DCM in small scintillation vials, which were placed inside a glass bottle containing diethyl ether. The product was then crystallized by dissolving it in DCM in small scintillation vials, which were placed inside a glass jar containing diethyl ether. The glass jar was capped and was placed in a freezer, and crystals (black blocks, 69%) formed through vapor diffusion. The crystals were filtered and dried under vacuum. Anal. Calcd for $C_{17}H_{19}NO_6ClS$: C, 50.94; H, 4.78; N, 3.49. Found: C, 50.91; H, 4.86; N, 3.36.

N-(2-(2-Methoxyethoxy)ethyl)phenothiazinium bis-(trifluoromethanesulfonyl)imide (MEEPT-TFSI). MEEPT (1.00 g, 3.32 mmol) was added to an oven-dried and cooled (to RT with a stream of nitrogen) 50 mL round-bottomed flask containing a stir bar. Anhydrous ACN (15 mL) was dispensed from resulting pale yellow solvent-dispensing system and the solution was stirred under nitrogen for the subsequent steps. Then, iodine (0.421 g, 1.66 mmol) and AgTFSI (1.31 g, 3.38 mmol) were added to the resulting solution. The reaction mixture turned dark orange and was stirred for 1 h, after which it was passed through a short pad of Celite. The filtrate was concentrated to approximately 2 mL total volume, after which diethyl ether (20 mL) was added, producing a dark precipitate. The resulting solid was washed with diethyl ether (20 mL) and hexanes (20 mL). The final precipitate was dried under vacuum to yield MEEPT-TFSI as a brownish black crystalline solid (1.75 g, 91%). The product was then crystallized by dissolving it in DCM in small scintillation vials, which were placed inside a glass jar containing diethyl ether. The glass jar was capped and was placed in a freezer, and crystals (greenish black rods, 81%) formed through vapor diffusion. The crystals were filtered and dried under vacuum. Anal. Calcd for $C_{19}H_{19}F_6N_2O_6S_3$: C, 39.24; H, 3.29; N, 4.82. Found: C, 39.21; H, 3.31; N, 4.87.

RESULTS AND DISCUSSION

Synthesis and Isolation of Crystalline MEEPT-X. Four radical cation salts of MEEPT were synthesized by chemical oxidation using nitrosonium salts $NOBF_4$ and $NOPF_6$, and the silver salts $AgClO_4 \cdot xH_2O$ and AgTFSI (Scheme 1). The use of nitrosonium salts is particularly attractive as the reduction product of these reagents is a gas (NO), meaning that no chemical reagents remain after the radical cation forms. For the synthesis of $TFSI^-$ and ClO_4^- salts of MEEPT, the respective silver salts were used in the presence of iodine to precipitate reduced silver as silver iodide, which was removed from the reaction mixture by filtration. The chemical reactions using these reagents proceed under mild conditions and are scalable; here, we scaled synthesis to produce 15−25 g batches of MEEPT-X. After preparing the salts, they were isolated as solids and further crystallized to produce X-ray quality crystals (Figure 1) by diffusion of diethyl ether into their solutions in DCM at low temperatures (ca −4 °C). The ability to crystallize these salts demonstrates their remarkable stability. The crystals of MEEPT-BF_4 are needle-shaped, MEEPT-PF_6 and MEEPT-ClO_4 are blocky, and MEEPT-TFSI crystals are rod-shaped, suggesting different packing motifs in the solid state. In all cases, the crystal systems are monoclinic, with space groups of $P2(1)/n$ for X = BF_4^- and PF_6^-, and $P2(1)/c$ for X = ClO_4^- and $TFSI^-$. The purity of crystalline salts was further demonstrated using CHN analysis. These salts were used for solution-state and solid-state studies.

Solution-State Stability Analysis. Electrochemical studies can be used to analyze the energetics and reversibility of redox events, giving information about the kinetics of electron transfer and the stability of charged states. In order to first assess the impact of these counteranions on the redox potential and on the chemical and electrochemical reversibility of the two oxidation events of MEEPT that are accessible in nonaqueous electrolytes, we used cyclic voltammetry (CV) and studied MEEPT (10 mM) in electrolytes containing 0.1 M Li-based salts in ACN. We chose ACN as the solvent for solution-state stability analysis as it is the most used organic solvent for nonaqueous RFB applications with desirable properties such as a broad stability window (>5 V), low viscosity (0.34 mPa s), and relative permittivity (35.9), offering opportunities for higher energy densities.[33] The results (Figure 2, Table 1, and Figure S1) show that the redox potential for the first oxidation varies only slightly with the counteranion, showing half-wave first oxidation potentials of 0.299−0.306 V versus ferrocene/ferrocenium ($Cp_2Fe^{0/+}$). The nature of the redox events also varies little with the identity of the supporting electrolyte, with species showing peak current ratios of 1.03−1.05 and peak separations of 56−62 mV. The results are more variable for the second oxidation, with greater reversibility being observed with PF_6^- and ClO_4^- than for BF_4^- and $TFSI^-$. These characteristics suggest that the dication of MEEPT is unstable in $LiBF_4$/ACN and LiTFSI/ACN but is persistent in $LiClO_4$/ACN and $LiPF_6$/ACN—at least on the experimental timescale (seconds) of the CV experiment.

https://dx.doi.org/10.1021/acs.chemmater.9b05345
Chem. Mater. 2020, 32, 3007−3017

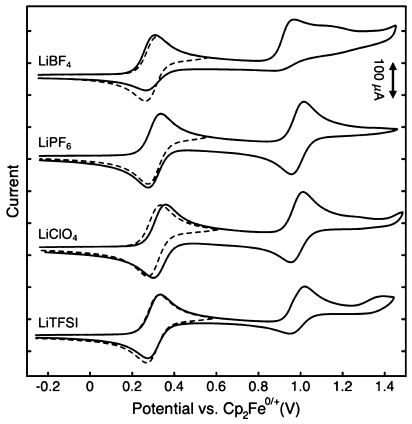

Figure 2. Cyclic voltammograms of 10 mM MEEPT in 0.1 M LiX/ACN where X = BF_4, PF_6, ClO_4, and TFSI, recorded at 100 mV/s and calibrated to $Cp_2Fe^{0/+}$ at 0 V. (See Figure S1 for voltammograms containing ferrocene as an internal reference).

Importantly, this result demonstrates how stability can be affected by the environment and suggests that MEEPT—which we previously treated as a one-electron donor for the purposes of cell cycling—might be utilized as a two-electron donor, given the appropriate combination of solvent and supporting salt.

Whereas CV is useful for screening the initial stability, it is insufficient as a technique used in isolation. As most applications require dissolution of radical cation salts in nonaqueous solvents, the stability of MEEPT-X in solution was studied by UV−vis spectroscopy and rotating RRDE.

UV−Vis Spectroscopy. UV−vis spectroscopy provides a straightforward stability analysis of organic compounds for energy storage applications, and a variety of concentrations can be analyzed, with upper and lower limits being determined by molar absorptivity of the species of interest. Phenothiazinium radical cations, for example, can be analyzed at the lowest concentrations by monitoring the most intensely absorbing peak at ca. 515 nm, with upper limits being determined by the intensity of the lower energy, less absorbing peaks at ca. 695, 770, and/or 860 nm.

We initially screened the stability of phenothiazinium salt solutions at concentrations of ca. 0.15−0.30 mM. Given that species decay was evident in only a few hours, yet phenothiazines show remarkable cycling stability at high concentrations,[11] we suspected that the decay we observed in UV−vis experiments was due to trace impurities in the solvent and that—as a result—this low concentration method was erroneously indicating species instability. Accordingly, we analyzed MEEPT-BF_4 at concentrations ranging from 0.1 to 10 mM in ACN, choosing the tetrafluoroborate salt because of it being the salt we had utilized in our previous symmetric cell studies. To prevent detector saturation, we analyzed solutions with concentrations of 1, 5, and 10 mM using a 0.1 cm path length cuvette versus a standard 1 cm cuvette used with concentrations of 0.1 and 0.5 mM. Figures 3a−e show the absorption spectra of MEEPT-BF_4 in ACN over a period of 3 h. For comparison of absorbance at different concentrations, a plot of absorbance versus time is shown in Figure 3f, with the absorption for each species at 5 min normalized to a value of 1 at 770 nm. At 0.1 mM, 82% of the initial intensity remained at 3 h, compared to 97, 97, 99, and 99% for concentrations of 0.5, 1, 5, and 10 mM. This result suggests that decay is indeed because of impurities in the solution. In an attempt to prevent trace impurities from affecting the results of the four radical cation salts, we chose to study the stability of MEEPT-X at 10 mM for further UV−vis analysis, as it negates the effect of trace impurities as well as allows analysis at a moderately high concentration that is compatible with the upper limit for CV studies and is at the lower limit of bulk electrolysis experiments.

The long-term stability of MEEPT-X in solution was studied using UV−vis spectroscopy to look for changes in intensity and/or formation of new peaks with time in the spectrum. Loss of intensity could arise from reduction of the radical cation salt to its neutral form, whereas changes in spectral shape would indicate the formation of new species. Solutions of MEEPT-X (10 mM) in ACN were inserted into 0.1 cm path length cuvettes, and analyzed weekly for 7 weeks. Figure 4 shows the absorption spectra over time for the four radical cation salts in ACN. We observed a decay in radical cation absorbance in all cases; however, the rate of decay varied with the counteranion identity. Figure 7a shows the normalized absorbance at 770 nm for samples recorded on different weeks, which is normalized against week 0 to plot versus time for total decay in absorbance. At week 7, the absorbance of MEEPT-BF_4 decreased the most (88%), followed by MEEPT-ClO_4 (69%), MEEPT-PF_6 (32%), and MEEPT-TFSI (20%). An increase in the higher energy (shorter wavelength) region was observed, which is consistent with the formation of neutral MEEPT. The results suggest that studying the radical cation absorbance profile over a period of a few hours is insufficient to compare different chemical environments. Longer-term stability analysis is therefore needed for stable radical cation salts when analyzed using UV−vis spectroscopy.

Rotating RRDE. The short-term stability of the electrochemically generated MEEPT radical cation was studied using RRDE shielding and collection experiments.[34] With these techniques, a known concentration of neutral MEEPT was dissolved in the electrolyte; the radical cation was initially

Table 1. Measured Half-Wave Potentials, Peak Separations, and Peak Current Ratios for the First and Second Oxidations of MEEPT at 10 mM in 0.1 M LiX-Based Electrolytes in ACN

	first oxidation ($E^{0/+}$)			second oxidation ($E^{+/2+}$)		
electrolyte	half-wave potential (V)	peak current ratios	peak separation (mV)	half-wave potential (V)	peak current ratios	peak separation (mV)
0.1 M $LiBF_4$/ACN	0.306	1.05	56	[a]	[a]	[a]
0.1 M $LiPF_6$/ACN	0.304	1.04	62	0.987	1.12	60
0.1 M $LiClO_4$/ACN	0.303	1.03	62	0.984	1.25	62
0.1 M LiTFSI/ACN	0.299	1.05	58	[a]	[a]	[a]

[a]Peak not analyzed because of its irreversibility.

https://dx.doi.org/10.1021/acs.chemmater.9b05345
Chem. Mater. 2020, 32, 3007−3017

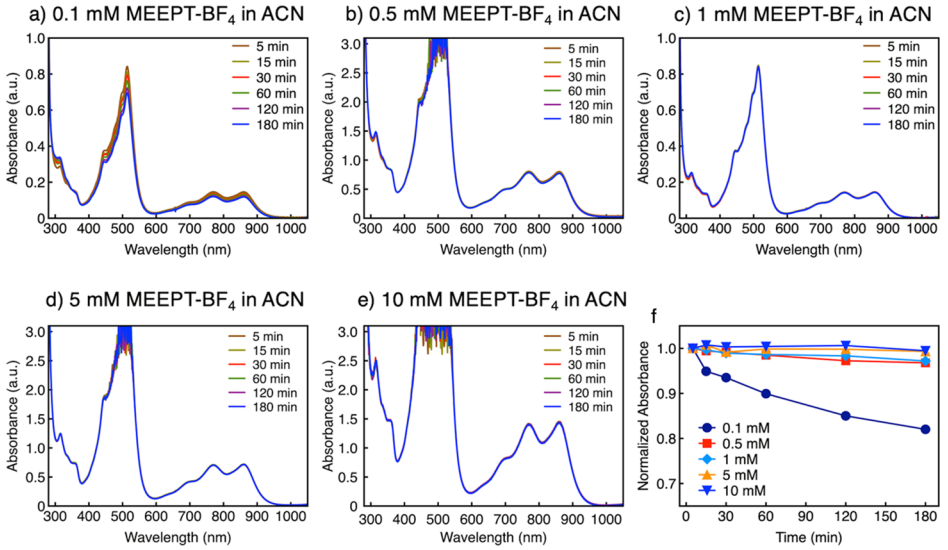

Figure 3. UV−vis spectra of MEEPT-BF_4 at (a) 0.1, (b) 0.5, (c) 1 (d) 5, (e) and 10 mM over time in ACN, recorded at 5, 15, 30, 60, 120, and 180 min after dissolution. Normalized absorbance of UV−vis absorbance at 770 nm vs time at various concentrations of MEEPT-BF_4 in ACN (f). Note: we are aware of the breakdown of the Beer−Lambert law at absorbance units of ca. 1.4−2.0 and only analyzed the decay of peaks with absorbance values of 1.5 or lower.

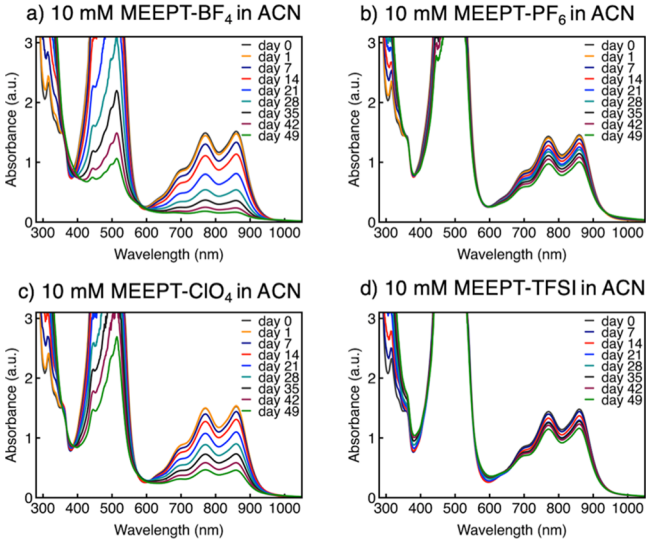

Figure 4. UV−vis spectra of 10 mM MEEPT-BF_4 (a), MEEPT-PF_6 (b), MEEPT-ClO_4 (c), and MEEPT-TFSI (d) in ACN, recorded at 5 min (day 0) after dissolution, after which spectra were recorded on days 0, 1, 7, 14, 21, 28, 35, 42, and 49.

absent. For each trial, two different protocols were run at each rotation rate sampled. First, the disk electrode was held at open-circuit voltage (OCV) while measuring the steady-state voltammogram at the ring electrode (from −0.2 to 0.9 V vs Ag/Ag^+). This ring current is denoted as "OCV". Second, chronoamperometry (CA) at the disk electrode results in MEEPT oxidation at a constant potential of 0.9 V versus Ag/Ag^+ while measuring the steady-state ring current. We denote this ring current as "CA". For a fully reversible reaction, the ring current shifts by a constant factor, $N_c i_{disk,lim}$, when the disk current is changed from 0 to a fixed, limiting current.[34] In other words, the difference between the limiting current regions of the OCV and CA curves should be constant if the MEEPT redox reaction is fully reversible. This relationship between ring currents is independent of the rotation rate or analyte concentration for a fully reversible reaction. When a reaction is not fully reversible, the difference between the two voltammograms is less than the constant value $N_c i_{disk,lim}$. The shielding percent, N_S, and collection efficiency, N_C, for a trial are calculated at each rotation rate according to the following

$$N_S = \frac{i^{ox}_{ring,OCV} - i^{ox}_{ring,CA}}{i_{disk,lim}}$$

$$N_C = \frac{i^{red}_{ring,OCV} - i^{red}_{ring,CA}}{i_{disk,lim}}$$

where $i^{ox}_{ring,OCV}$ is the average limiting oxidation ring current when the disk is at OCV, $i^{ox}_{ring,CA}$ is the average limiting oxidation ring current when the disk is performing CA, $i^{red}_{ring,OCV}$ is the average limiting reduction ring current when the disk is at OCV, $i^{red}_{ring,CA}$ is the average limiting reduction ring current when the disk is performing CA, and $i_{disk,lim}$ is the average limiting disk current while performing CA at 0.9 V versus Ag/Ag^+.

Steady-state ring voltammograms at concentrations of 0.1−250 mM were collected in 0.1 M $TEABF_4$ in ACN, with $TEABF_4$ being selected because of our common employment of this salt in flow cell cycling experiments. The results are shown in Figure 5a−e, and a comparison of calculated collection efficiencies, N_C, at concentrations of 0.1−250 mM is shown in Figure 5f. At low concentrations of MEEPT (0.1 and 0.5 mM, Figure 5a,b), the measured ring currents in the limiting current potential windows are not flat, indicating background current at these high potentials because of electrolyte or impurity oxidation. This background current is only detected when the current attributed to MEEPT oxidation is low, because at moderate MEEPT concentrations (10 mM, Figure 5c), the voltammograms show flat limiting current regions. At high concentrations (100 and 250 mM, Figure 5d,e), the oxidative current shows linear behavior consistent with a high ohmic resistance. At these concentrations, the concentration of MEEPT is similar to that of the electrolyte salt. In this concentration regime, $TEABF_4$ is not an

https://dx.doi.org/10.1021/acs.chemmater.9b05345
Chem. Mater. 2020, 32, 3007−3017

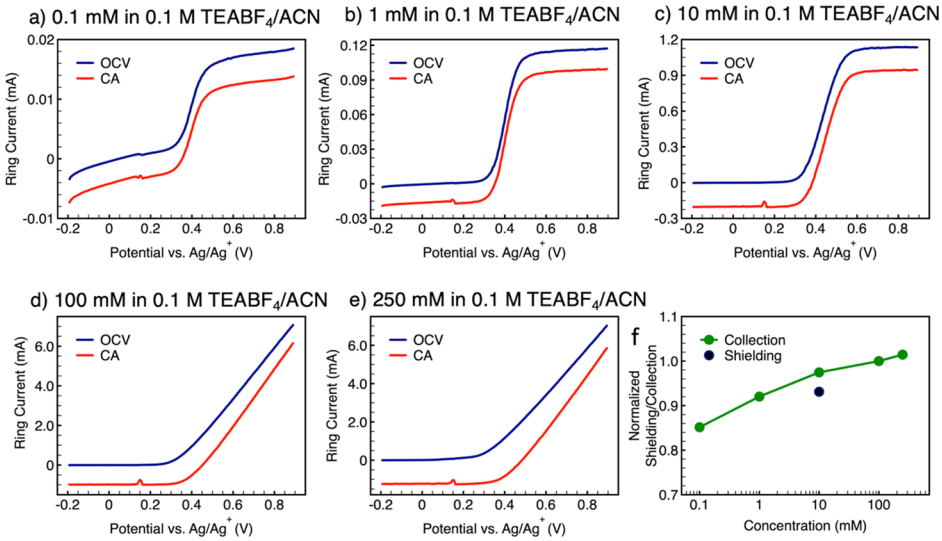

Figure 5. Steady-state ring current with a disk at the open circuit (blue) and with a disk at the anodic limiting current (red) for MEEPT at 0.1 (a), 1 (b), 10 (c), 100 (d), and 250 mM (e) in 0.1 M $TEABF_4$/ACN. (f) Voltammograms collected at a 100 mV/s scan rate and 900 rpm rotation rate. Summary of the collection efficiency and shielding percent, normalized to the geometric limit (27.6%) shown.

effective supporting electrolyte, and the electric field in solution affects the transport of $MEEPT^{+\bullet}$. Migration significantly complicates the transport, and the simplified analysis of ref 34 can no longer be applied. In Figure 5f, the shielding percent is not reported for low and high MEEPT concentrations because of these parasitic currents and high ohmic resistance, respectively. Figure 5f shows that even when these effects can be neglected, the calculated collection efficiency increases with increasing MEEPT concentration, demonstrating that the $MEEPT^{+\bullet}$ radical cation is least stable at low concentrations.

As previously mentioned, the instability of $MEEPT^{+\bullet}$ at low concentrations is inconsistent with its previous cycling performance in RFBs at concentrations of ca. 0.4 M. To determine whether trace water was responsible for self-discharge and/or decomposition, 500−5000 ppm water was added to a solution of 10 mM MEEPT in 0.1 M LiTFSI—the most stable supporting electrolyte. The voltammograms (Figure S3a) were indiscernible from water-free samples, and the calculated shielding and collection efficiencies (Figure S3b) showed no impact of water. Thus, whereas impurities likely limit the solution-phase degradation of the radical cation, water is unlikely to play a significant role.

Steady-state ring voltammograms were collected for 10 mM MEEPT in various electrolytes containing 0.1 M conductive salt in ACN. These results for Li-containing electrolytes (Figure 6) and other conductive salt cations (Figure S2) are summarized in Figure 7b. Voltammograms collected for $LiBF_4$ and $LiClO_4$ electrolytes show greater ring currents (Figure 6a,c, respectively) than for $LiPF_6$ and LiTFSI electrolytes (Figure 6b,d, respectively), and the disk-limiting currents (not shown) are also larger in these electrolytes. This hints that the diffusivity of MEEPT is faster in the presence of BF_4^- and ClO_4^-, when compared to PF_6^- and $TFSI^-$; however, the difference in calculated diffusivities is small. Interestingly, comparing the calculated average collection and shielding efficiencies for these electrolytes in Figure 7b shows that $MEEPT^{+\bullet}$ is more stable in an LiTFSI-based electrolyte than in an $LiClO_4$-based electrolyte.

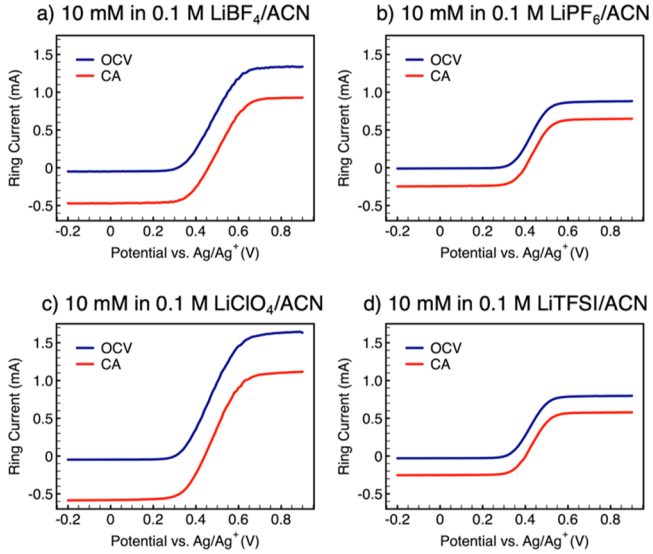

Figure 6. Steady-state ring current with a disk at the open circuit (blue) and with a disk at the anodic limiting current (red) for MEEPT at 10 mM in 0.1 M $LiBF_4$/ACN (a), 0.1 M $LiPF_6$/ACN (b), 0.1 M $LiClO_4$/ACN (c), and 0.1 M LiTFSI/ACN (d). Voltammograms were collected at a scan rate of 100 mV/s and a rotation rate of 900 rpm.

Comparison of UV−Vis and RRDE Techniques. Figure 7 shows a comparison of the results obtained from UV−vis experiments versus those from RRDE. Figure 7a shows the absorption intensity at each week for over 7 weeks. As previously mentioned, Figure 7b shows a summary of the RRDE results for all electrolytes studied, including those shown in Figure 6. Figure 7b presents the average collection and shielding percentages calculated for three trials of each electrolyte over three rotation rates (400, 900, and 1600 rpm). Error bars in Figure 7b represent one standard deviation from the mean over three trials. Although the timescales of the experiments differ by orders of magnitude and the presence of the supporting electrolyte, both the techniques essentially lead to the same conclusion, predicting that MEEPT-TFSI is the

https://dx.doi.org/10.1021/acs.chemmater.9b05345
Chem. Mater. 2020, 32, 3007−3017

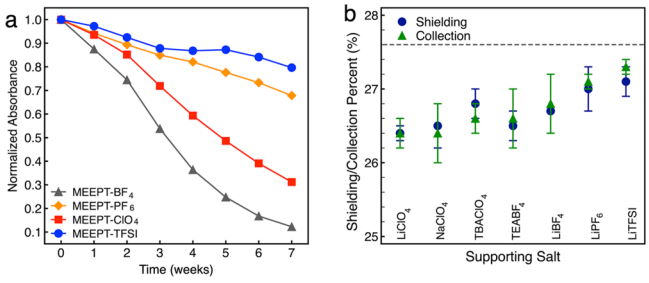

Figure 7. (a) Normalized intensity of UV−vis absorbance at 770 nm of 10 mM MEEPT-X salts over time in ACN, recorded at 5 min (0 week) after dissolution, after which the same solutions were recorded on 1, 2, 3, 4, 5, 6, and 7 weeks. (b) Average shielding and collection percent over different rpm for 10 mM MEEPT in 0.1 M salt in ACN electrolytes. Error bars represent 1 standard deviation from the mean for three trials. The dashed line indicates the geometric limit for a perfectly stable reaction.

most stable among all salts. However, RRDE leads to this conclusion faster than UV−vis. RRDE also shows that some of the $MEEPT^{+\bullet}$ instability is due to the reversible formation of neutral MEEPT, whereas some is due to irreversible decomposition. Quantifying the relative fractions of each pathway under different conditions is the focus of ongoing work.

Figures 5, 6, and 7b demonstrate the advantages of using a rotating ring-disk electrode, generator-collector methodology, to study radical cation stability. The radical cation is generated and measured in situ; thus, molecular stability is studied under similar conditions to those encountered in electrochemical energy storage systems that contain electrolyte salts dissolved in nonaqueous solvents, such as LIBs and RFBs. This technique also quickly screens active molecules in various chemical environments and across a range of concentrations. Controlling the rotation rate can also vary the convective time constant between electrodes to determine the kinetic information on cation decomposition reactions. However, Figure 5 also demonstrates certain limitations of this approach: at high active molecule concentrations, the ohmic potential drop obscures the oxidative limiting current and prevents calculating a shielding percent at high concentrations. Overall, the RRDE generator-collector methodology is advantageous for quickly screening the radical cation stability at low and moderate concentrations applicable to nonaqueous RFBs.

Solid-State Stability Analysis of MEEPT-X. In addition to knowing how electrolyte salts and counterions affect the stability of the MEEPT radical cation in solution, we were interested in how counterions affect the solid-state stability, as the solid-state stability dictates how these should be stored in order to not lose activity with time, especially for the design of shelf-stable reagents. Thus, we examined the shelf life and thermal stability of MEEPT-X in the solid state with varying counteranions. Comparing salts stored on the benchtop versus inside a glovebox gives an idea of their stability to oxygen and moisture, and would inform us of whether our precautionary measures of always storing MEEPT radical cations salts in our glove box is necessary.

To analyze the shelf-life stability, samples of crystalline MEEPT-X were stored in vials that were kept on the benchtop as well as in an argon-filled glovebox. The stability analysis was done using UV−vis spectroscopy. A 10 mM sample of each salt was prepared and UV−vis spectra recorded in ACN at days 0, 1, 7, 14, and 21. The absorbance of the radical cation was again monitored to look for changes in intensity and/or formation of new peaks with time in the spectrum (Figures 8 and S4), which

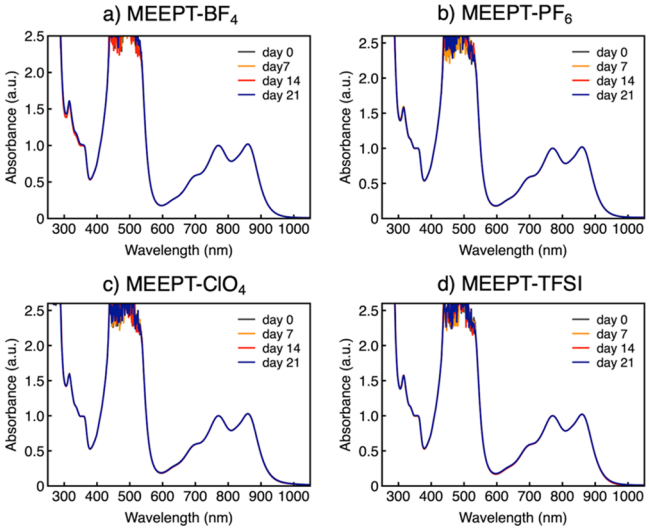

Figure 8. UV−vis spectra (normalized at 770 nm) of 10 mM MEEPT-BF_4 (a), MEEPT-PF_6 (b), MEEPT-ClO_4 (c), and MEEPT-TFSI (d), which were prepared at 1-week intervals from crystalline samples stored in glass vials kept on the benchtop.

would indicate decomposition. The absorbance at 770 nm for each day was normalized and plotted against the wavelength. No appreciable difference in shape and intensity in the MEEPT-X UV−vis spectrum was observed regardless of whether the salts were stored under ambient (Figure 8) or inert atmosphere (Figure S4) over a period of 21 days. The analysis suggested that all MEEPT salts under consideration are stable in ambient conditions, which—unlike solution-state stability—is independent of the identity of the counteranion.

The thermal stability of each crystalline salt was first accessed using thermogravimetric analysis (Figure 9). The salts

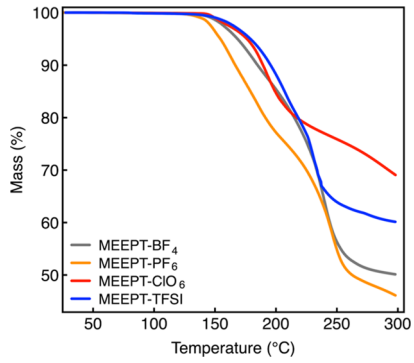

Figure 9. Thermal stability of MEEPT-X measured using thermogravimetric analysis under air, with the temperature increasing from RT to 300 °C at a rate of 10 °C min^{-1}.

were heated from RT to 300 °C under air at a rate of 10 °C/min. At this rate of heating, the salts of MEEPT showed a similar thermal stability, with all being stable at least until 140 °C after which weight loss was observed. The shape of the weight loss curve and the amount of residue left at 300 °C varied with the counteranion. We compared the amount of residue versus the percent of anion present and found that the

https://dx.doi.org/10.1021/acs.chemmater.9b05345
Chem. Mater. 2020, 32, 3007−3017

mass loss does not correlate with the percent of anion present in the salt (Table 2). At this time, we are unsure what species remain after heating to these high temperatures.

Table 2. Onset Temperature of Weight Loss and Residue from TGA of MEEPT-X Heated from RT to 300 °C at a Rate of 10 °C min^{-1} in Air

compound	onset temperature of weight loss (°C)[a]	% anion in original salt	% residue at 300 °C
MEEPT-BF_4	147	22	50
MEEPT-PF_6	138	32	46
MEEPT-ClO_4	150	25	69
MEEPT-TFSI	151	48	60

[a]The temperature listed is that at which the sample lost 1% of its original mass.

In order to study the extended thermal stability of MEEPT-X at intermediate temperatures for longer durations, we analyzed the stability of crystals heated at various temperatures overnight. The samples were stored in uncapped glass vials and stored at 30, 50, 70, and 90 °C in ambient atmosphere. Photographs of the samples after storage are shown in Figure 10a. Unstable salts formed a melt at higher temperatures. The

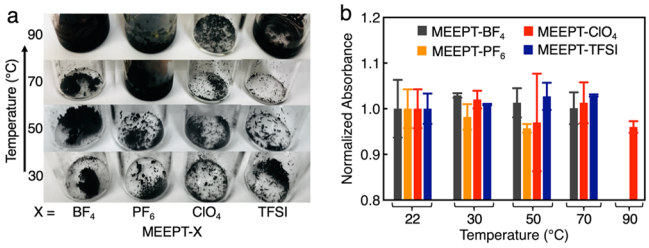

Figure 10. (a) Photographs of the crystals of MEEPT-X salts after storage overnight at 30, 50, 70, and 90 °C. (b) Normalized intensity of UV−vis absorbance at 770 nm vs temperature of MEEPT-X kept overnight at RT, 30, 50, 70, and 90 °C. To obtain UV−vis spectra, a 10 mM solution in ACN was freshly prepared and UV−vis spectra were recorded.

stability at each temperature was analyzed using UV−vis spectroscopy. A measured amount of solid was weighed to make a solution at 10 mM in ACN; its absorption spectrum was compared to samples kept at RT (22 °C). Figure 10b shows a comparison of the thermal stability of MEEPT-X under air at different temperatures based on absorption intensities. MEEPT-PF_6 was the least stable, only surviving overnight at 50 °C. MEEPT-BF_4, MEEPT-TFSI, and MEEPT-ClO_4 all survived overnight at 70 °C. Only MEEPT-ClO_4 remained stable when heated overnight at 90 °C.

Figure 11 shows the original UV−vis spectra of MEEPT-X solutions prepared from solid samples stored at different temperatures. At temperatures at which crystalline salts were still solids, the absorption profile remained similar to the samples kept at RT. For salts that showed phase changes at higher temperatures, the UV−vis spectra changed shape significantly, becoming broader and absorbing at lower energies than the original salts, which could be due to the formation of oligomeric/polymeric species.

Analysis of the Decomposition Products of MEEPT-X. Previously, we characterized the decomposition reactions of phenothiazines in battery electrolytes, specifically 1.2 M $LiPF_6$ in ethylene carbonate/ethyl methyl carbonate (3/7 wt ratio).

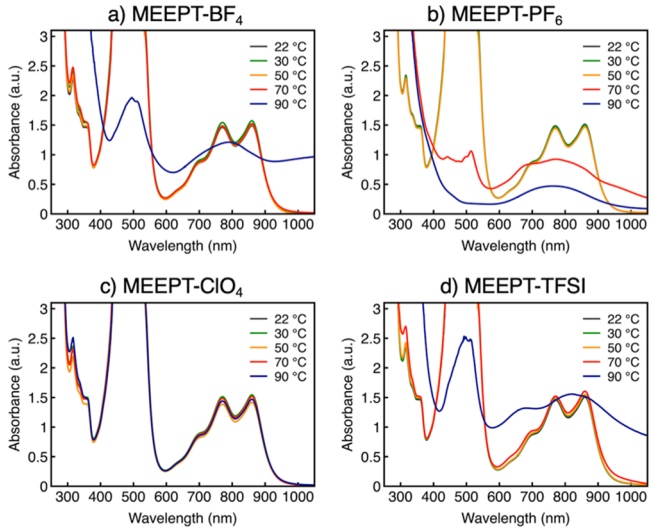

Figure 11. UV−vis spectra of MEEPT-BF_4 (a), MEEPT-PF_6 (b), MEEPT-ClO_4 (c), and MEEPT-TFSI (d) dissolved in ACN after storage in ambient atmosphere overnight at 22, 30, 50, 70, and 90 °C.

The phenothiazines acted as redox shuttles for overcharge mitigation by cycling through their neutral and radical cation forms.[20,35] We observed that the identity of the alkyl group in N-substituted phenothiazines can significantly alter the stability of the radical cation form. Derivatives underwent C−N bond cleavage to varying extents, forming the parent, unsubstituted phenothiazine radical cation, which is subject to further oligomerization. Further reactions observed for stable phenothiazine redox shuttles in these carbonate-based battery electrolytes included the transformation of the thioether to form a sulfone or a sulfoxide—a reaction that requires a source of oxygen—forming new chemical species with higher oxidation potentials.

Curious if we would see similar decomposition routes in ACN-based solutions, we analyzed 7-week-old MEEPT-BF_4/ACN solutions using ^{1}H NMR spectroscopy. We first quenched the remaining radical cations (a paramagnetic species) by addition of sodium thiosulfate, then filtered the solution to remove sodium-containing solids, and concentrated the sample to remove ACN. The concentrated extracts were then dissolved in DMSO-d_6 and ^{1}H NMR spectra were recorded (see the aromatic region in Figure 12b, and an expansion in Figure S5). For comparison, a freshly prepared solution of MEEPT-BF_4 in ACN was quenched and analyzed by ^{1}H NMR (Figures 12a and S5). The nuclear magnetic resonance (NMR) spectrum of the aged sample (note the aromatic region, ca. 6−8 ppm) shows the presence of MEEPT. Additionally, less intense peaks were also observed in the aromatic and aliphatic regions, indicating (~10%) partial decomposition. Further investigation of byproduct formation in the solution state is underway.

Previous efforts to determine the effects of counterion identity on stability are limited. In one notable example, the stability of triarylaminium radical cations in solution and in the solid state was found to vary with the counterion. Solutions of tris-(*p*-bromophenyl)aminium hexachloroantimonate in DCM were more stable than the perchlorate form when measured over several days; no reason for the varying stability was proposed.[36] In the solid state, the PF_6^-, $SbCl_6^-$, and WCl_6^- salts of tris-(*p*-bromophenyl)ammonium cations showed little

https://dx.doi.org/10.1021/acs.chemmater.9b05345
Chem. Mater. 2020, 32, 3007−3017

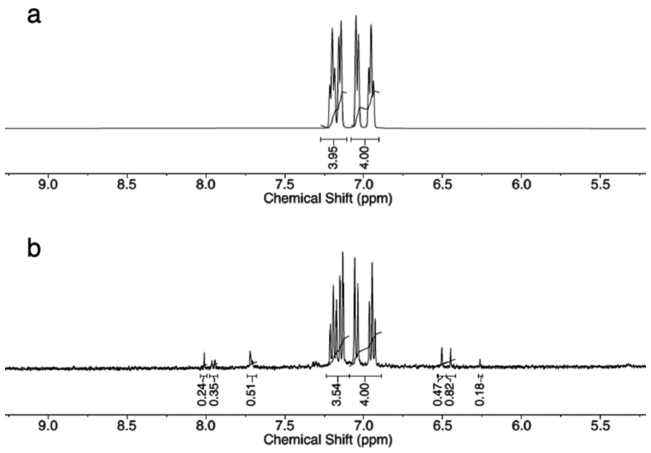

Figure 12. Aromatic region of ^{1}H NMR spectra of freshly prepared (a) and 7-week-old (b) MEEPT-BF_4/ACN solutions, concentrated and redissolved in DMSO-d_6 after reduction to their neutral form by treatment with sodium thiosulfate.

deterioration compared to the equivalent BF_4^- salt, which more rapidly dibrominated to form benzidine species.[37,38] By contrast, all MEEPT-X salts were stable under ambient conditions in the solid state for the observed time period of 3 weeks.

To determine the reaction outcomes from solid MEEPT-BF_4, MEEPT-PF_6, and MEEPT-TFSI heated to 90 °C, we analyzed samples using ESI−MS (Figures 13 and S6). The

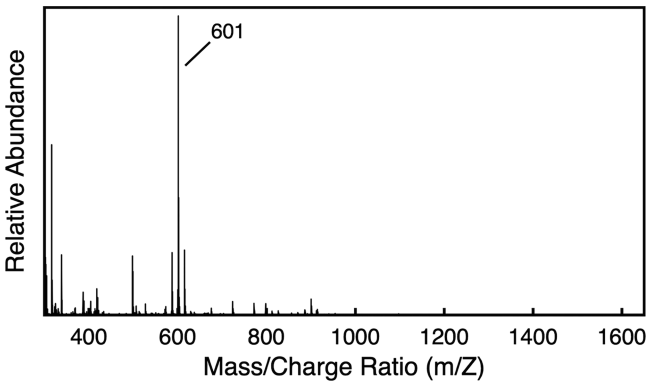

Figure 13. ESI−MS in positive-ion mode of the materials present after heating MEEPT-TFSI in the solid state at 90 °C overnight.

analyses surveyed a wide m/z scan (300−2000) to look for the formation of fragments, adducts, and polymerized byproducts of MEEPT in positive-ion and negative-ion modes. The mass spectra for thermally treated MEEPT-TFSI (Figure 13) contain similar features to that of the BF_4^- and PF_6^- salts. In positive-ion mode, mass spectra of all three salts show peaks at around m/z 316, 601, and 900, with 601 being the most abundant. The peaks at m/z 601 and 900 likely correspond to dimers and trimers of MEEPT (301 g/mol).

Dimers and higher oligomers are formed by reaction of MEEPT radicals at the positions para to the nitrogen atoms (Scheme 2). This is a common decomposition mechanism observed in aromatic amines, such as triphenylamines, in their radical cation forms.[39−41] Phenothiazine can oxidatively polymerize to form polyphenothiazine, where the chain propagation occurs at the carbon atoms para to the phenothiazine nitrogen.[42] The delocalized nature of phenothiazine radicals is represented by two resonance structures, which are shown in Scheme 2 with a double-headed arrow. Additionally, because we have observed self-discharge of the radical cation, we represented this process as donation of an electron to yield the neutral form. An investigation to determine the identity of the reducing agent(s) is underway.

CONCLUSIONS

Radical cation salts of the glycolated phenothiazine derivative MEEPT can be isolated as crystalline solids after chemically oxidizing the neutral compound with NO-X and Ag-X reagents. By synthesizing four different salts, with counterions BF_4^-, PF_6^-, ClO_4^-, and $TFSI^-$, we were able to determine the effect of counterion identity on the stability of the MEEPT radical cation in solution and in the solid state. Solid-state stability trends required heating the samples to >70−140 °C, regardless of the counterion; the need for these temperatures illustrates their incredible stability in the solid state. Whether stored in an argon atmosphere glove box or on the benchtop, samples showed no indication of decay after 3 weeks of analysis. This result indicates that MEEPT-X samples do not have to be protected in inert atmosphere, allowing for benchtop handling of this material.

Importantly, the long-term solution-based stability results from UV−vis measurements showed similar trends to solution-based stability results from rotating RRDE, indicating that RRDE can be used to rapidly screen for stability over seconds or minutes instead of several weeks via UV−vis. An additional advantage of RRDE is that it can be used to determine whether a molecule is irreversibly decomposed versus reversibly self-discharged. The greatest disadvantage of RRDE is the limited concentration of MEEPT that can be analyzed. At higher concentrations of the redox-active molecule (0.1 M and higher in this study), large ohmic losses and migration effects on transport limit the applicability of standard analytical expressions.

Scheme 2. Self-Discharge Through Electron Transfer Leads to the Formation of Neutral MEEPT in the Solution State, and the Thermal Decomposition of the MEEPT Radical Cation in Solid State to a Phenothiazine Dimer

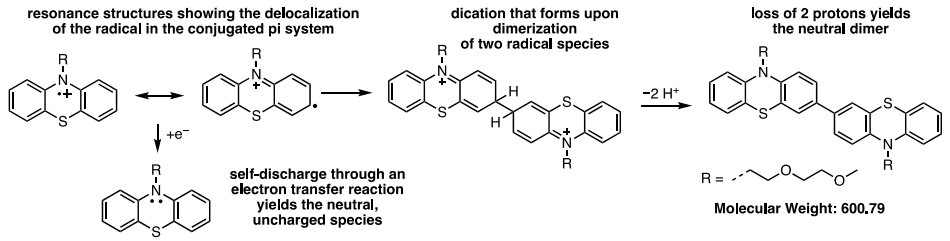

https://dx.doi.org/10.1021/acs.chemmater.9b05345
Chem. Mater. 2020, 32, 3007−3017

Whereas we do not yet understand the mechanistic origins of stability trends with different counterions, it is important to note the distinction between trends in solution and in the solid state. In the solution state, a long-term UV−vis analysis indicates that stability trends as $TFSI^- > PF_6^- > ClO_4^- > BF_4^-$, and with RRDE as $TFSI^- > PF_6^- > BF_4^- > ClO_4^-$. These results contrast with the solid-state thermal stability trends of $ClO_4 > BF_4 \approx TFSI > PF_6$. This result underscores the need to match the stability testing conditions to the desired application, be it storage and transport (solid-state) or deployment (solution). Ongoing work to improve the stability of MEEPT-X will focus on identifying the decomposition pathways in solution, including the effects of electrolyte impurities. Improved the understanding of these reactions will enable electrolyte design to extend the lifetimes of MEEPT and other electron-donating materials for electrochemical energy storage systems.

■ ASSOCIATED CONTENT

Supporting Information

The Supporting Information is available free of charge at https://pubs.acs.org/doi/10.1021/acs.chemmater.9b05345.

X-ray crystallographic data of MEEPT-BF_4(CIF)
X-ray crystallographic data of MEEPT-PF_6 (CIF)
X-ray crystallographic data MEEPT-$Cl0_4$ (CIF)
X-ray crystallographic data MEEPT-TFSI (CIF)
Cyclic voltammograms, rotating ring disk electrode voltammetry, UV−vis, NMR spectra, and mass spectra (PDF)

■ AUTHOR INFORMATION

Corresponding Authors

Maureen H. Tang − *Department of Chemical & Biological Engineering, Drexel University, Philadelphia, Pennsylvania 19104, United States;* orcid.org/0000-0003-0037-4814; Email: mhtang@drexel.edu

Susan A. Odom − *Department of Chemistry, University of Kentucky, Lexington, Kentucky 40506, United States; Joint Center for Energy Storage Research, Lexington, Kentucky 40506, United States;* orcid.org/0000-0001-6708-5852; Email: susan.odom@uky.edu

Authors

Aman Preet Kaur − *Department of Chemistry, University of Kentucky, Lexington, Kentucky 40506, United States; Joint Center for Energy Storage Research, Lexington, Kentucky 40506, United States;* orcid.org/0000-0001-7617-8137

Oliver C. Harris − *Department of Chemical & Biological Engineering, Drexel University, Philadelphia, Pennsylvania 19104, United States;* orcid.org/0000-0002-5484-5688

N. Harsha Attanayake − *Department of Chemistry, University of Kentucky, Lexington, Kentucky 40506, United States; Joint Center for Energy Storage Research, Lexington, Kentucky 40506, United States;* orcid.org/0000-0002-1741-8847

Zhiming Liang − *Department of Chemistry, University of Kentucky, Lexington, Kentucky 40506, United States;* orcid.org/0000-0001-6185-0605

Sean R. Parkin − *Department of Chemistry, University of Kentucky, Lexington, Kentucky 40506, United States;* orcid.org/0000-0001-5777-3918

Complete contact information is available at: https://pubs.acs.org/10.1021/acs.chemmater.9b05345

Notes

The authors declare the following competing financial interest(s): The University of Kentucky has a licensing agreement with Tokyo Chemicals, Inc. who manufactures and sells MEEPT.

■ ACKNOWLEDGMENTS

The Odom group thanks the Department of Energy, Office of Science, Basic Energy Sciences for funding through the Joint Center for Energy Storage Research for support of solution-based stability studies, and thanks the National Science Foundation for support through CHE CSDM-B (award number 1800482) for solid-state stability studies. APK thanks Mark Crocker and Robert Pace at the University of Kentucky for access to their TGA instrument. The Tang group thanks the National Science Foundation for support through the CBET division (award number 1751553) for RRDE experiments. SRP thanks the NSF MRI program (award number 1625732) for support for the purchase of an X-ray diffractometer.

■ REFERENCES

(1) Schon, T. B.; McAllister, B. T.; Li, P.-F.; Seferos, D. S. The rise of organic electrode materials for energy storage. *Chem. Soc. Rev.* **2016**, *45*, 6345−6404.

(2) Winsberg, J.; Hagemann, T.; Janoschka, T.; Hager, M. D.; Schubert, U. S. Redox-Flow Batteries: From Metals to Organic Redox-Active Materials. *Angew. Chem., Int. Ed.* **2017**, *56*, 686−711.

(3) Stolar, M.; Baumgartner, T. Organic n-type materials for charge transport and charge storage applications. *Phys. Chem. Chem. Phys.* **2013**, *15*, 9007−9024.

(4) Liu, Y.; Goulet, M.-A.; Tong, L.; Liu, Y.; Ji, Y.; Wu, L.; Gordon, R. G.; Aziz, M. J.; Yang, Z.; Xu, T. A Long Lifetime All-Organic Aqueous Flow Battery Utilizing TMAP-TEMPO Radical. *Chem* **2019**, *5*, 1861−1870.

(5) Sevov, C. S.; Samaroo, S. K.; Sanford, M. S. Cyclopropenium Salts as Cyclable, High-Potential Catholytes in Nonaqueous Media. *Adv. Energy Mater.* **2017**, *7*, 1602027−1602032.

(6) Vaid, T. P.; Sanford, M. S. An Organic Super-Electron-Donor as a High Energy Density Negative Electrolyte for Nonaqueous Flow Batteries. *Chem. Commun.* **2019**, *55*, 11037−11040.

(7) Hollas, A.; Wei, X.; Murugesan, V.; Nie, Z.; Li, B.; Reed, D.; Liu, J.; Sprenkle, V.; Wang, W. A Biomimetic High-capacity Phenazine-Based Anolyte for Aqueous Organic Redox Flow Batteries. *Nat. Energy* **2018**, *3*, 508−514.

(8) Wei, X.; Xu, W.; Vijayakumar, M.; Cosimbescu, L.; Liu, T.; Sprenkle, V.; Wang, W. TEMPO-Based Catholyte for High-Energy Density Nonaqueous Redox Flow Batteries. *Adv. Mater.* **2014**, *26*, 7649−7653.

(9) Huang, J.; Su, L.; Kowalski, J. A.; Barton, J. L.; Ferrandon, M.; Burrell, A. K.; Brushett, F. R.; Zhang, L. A subtractive approach to molecular engineering of dimethoxybenzene-based redox materials for non-aqueous flow batteries. *J. Mater. Chem. A* **2015**, *3*, 14971−14976.

(10) DeBruler, C.; Hu, B.; Moss, J.; Liu, X.; Luo, J.; Sun, Y.; Liu, T. L. Designer Two-Electron Storage Viologen Anolyte Materials for Neutral Aqueous Organic Redox Flow Batteries. *Chem* **2017**, *3*, 961−978.

(11) Milshtein, J. D.; Kaur, A. P.; Casselman, M. D.; Kowalski, J. A.; Modekrutti, S.; Zhang, P. L.; Harsha Attanayake, N.; Elliott, C. F.; Parkin, S. R.; Risko, C.; Brushett, F. R.; Odom, S. A. High Current Density, Long Duration Cycling of Soluble Organic Active Species for Non-Aqueous Redox Flow Batteries. *Energy Environ. Sci.* **2016**, *9*, 3531−3543.

(12) Hoober-Burkhardt, L.; Krishnamoorthy, S.; Yang, B.; Murali, A.; Nirmalchandar, A.; Prakash, G. K. S.; Narayanan, S. R. A New Michael-Reaction-Resistant Benzoquinone for Aqueous organic Redox Flow Batteries. *J. Electrochem. Soc.* **2017**, *164*, A600−A607.

(13) Yang, Z.; Tong, L.; Tabor, D. P.; Beh, E. S.; Goulet, M.-A.; De Porcellinis, D.; Aspuru-Guzik, A.; Gordon, R. G.; Aziz, M. J. Alkaline Benzoquinone Aqueous Flow Battery for Large-Scale Storage of Electrical Energy. *Adv. Energy Mater.* **2018**, *8*, 1702056.
(14) Cao, J.; Tao, M.; Chen, H.; Xu, J.; Chen, Z. A Highly Reversible Anthraquinone-based Anolyte for Alkaline aqueous Redox Flow Batteries. *J. Power Sources* **2018**, *386*, 40−46.
(15) Kwon, G.; Lee, S.; Hwang, J.; Shim, H.-S.; Lee, B.; Lee, M. H.; Ko, Y.; Jung, S.-K.; Ku, K.; Hong, J.; Kang, K. Multi-redox Molecule for High-Energy Redox Flow Batteries. *Joule* **2018**, *2*, 1771−1782.
(16) Yan, Y.; Robinson, S. G.; Sigman, M. S.; Sanford, M. S. Mechanism-Based Design of a High-Potential Catholyte Enables a 3.2 V All-Organic Nonaqueous Redox Flow Battery. *J. Am. Chem. Soc.* **2019**, *141*, 15301−15306.
(17) Hendriks, K. H.; Sevov, C. S.; Cook, M. E.; Sanford, M. S. Multielectron Cycling of a Low-Potential Anolyte in Alkali Metal Electrolytes for Nonaqueous Redox Flow Batteries. *ACS Energy Lett.* **2017**, *2*, 2430−2435.
(18) Hu, B.; Liu, T. L. Two Electron Utilization of Methyl Viologen Anolyte in Nonaqueous Organic Redox Flow Battery. *J. Energy Chem.* **2018**, *27*, 1326−1332.
(19) Attanayake, N. H.; Kowalski, J. A.; Greco, K. V.; Casselman, M. D.; Milshtein, J. D.; Chapman, S. J.; Parkin, S. R.; Brushett, F. R.; Odom, S. A. Tailoring Two-Electron-Donating Phenothiazines To Enable High-Concentration Redox Electrolytes for Use in Non-aqueous Redox Flow Batteries. *Chem. Mater.* **2019**, *31*, 4353−4363.
(20) Casselman, M. D.; Kaur, A. P.; Narayana, K. A.; Elliott, C. F.; Risko, C.; Odom, S. A. The fate of phenothiazine-based redox shuttles in lithium-ion batteries. *Phys. Chem. Chem. Phys.* **2015**, *17*, 6905−6912.
(21) Huang, J.; Pan, B.; Duan, W.; Wei, X.; Assary, R. S.; Su, L.; Brushett, F. R.; Cheng, L.; Liao, C.; Ferrandon, M. S.; Wang, W.; Zhang, Z.; Burrell, A. K.; Curtiss, L. A.; Shkrob, I. A.; Moore, J. S.; Zhang, L. The Lightest Organic Radical Cation for Charge Storage in Redox Flow Batteries. *Sci. Rep.* **2016**, *6*, 32102−32111.
(22) Sevov, C. S.; Brooner, R. E. M.; Chénard, E.; Assary, R. S.; Moore, J. S.; Rodríguez-López, J.; Sanford, M. S. Evolutionary design of low molecular weight organic anolyte materials for applications in nonaqueous redox flow batteries. *J. Am. Chem. Soc.* **2015**, *137*, 14465−14472.
(23) Wei, X.; Xu, W.; Huang, J.; Zhang, L.; Walter, E.; Lawrence, C.; Vijayakumar, M.; Henderson, W. A.; Liu, T.; Cosimbescu, L.; Li, B.; Sprenkle, V.; Wang, W. Radical Compatibility with Nonaqueous Electrolytes and Its Impact on an All-Organic Redox Flow Battery. *Angew. Chem., Int. Ed.* **2015**, *54*, 8684−8687.
(24) Kaur, A. P.; Holubowitch, N. E.; Ergun, S.; Elliott, C. F.; Odom, S. A. A Highly Soluble Organic Catholyte for Non-Aqueous Redox Flow Batteries. *Energy Technol.* **2015**, *3*, 476−480.
(25) Kowalski, J. A.; Casselman, M. D.; Kaur, A. P.; Milshtein, J. D.; Elliott, C. F.; Modekrutti, S.; Attanayake, N. H.; Zhang, N.; Parkin, S. R.; Risko, C.; Brushett, F. R.; Odom, S. A. A Stable Two-Electron-Donating Phenothiazine for Application in Nonaqueous Redox Flow Batteries. *J. Mater. Chem. A* **2017**, *5*, 24371−24379.
(26) Zhang, J.; Yang, Z.; Shkrob, I. A.; Assary, R. S.; Tung, S. O.; Silcox, B.; Duan, W.; Zhang, J.; Su, C. C.; Hu, B.; Pan, B.; Liao, C.; Zhang, Z.; Wang, W.; Curtiss, L. A.; Thompson, L. T.; Wei, X.; Zhang, L. Annulated Dialkoxybenzenes as Catholyte Materials for Non-aqueous Redox Flow Batteries: Achieving High Chemical Stability through Bicyclic Substitution. *Adv. Energy Mater.* **2017**, *7*, 1701272.
(27) Jia, X. Radical Cation Salts: From Single-Electron Oxidation to C−H Activation. *Synthesis* **2016**, *48*, 18−30.
(28) Steckhan, E. Indirect Electroorganic Syntheses—A Modern Chapter of Organic Electrochemistry [New Synthetic Methods (59)]. *Angew. Chem., Int. Ed. Engl.* **1986**, *25*, 683−701.
(29) Armstrong, C. G.; Toghill, K. E. Stability of molecular radicals in organic non-aqueous redox flow batteries: A mini review. *Electrochem. Commun.* **2018**, *91*, 19−24.
(30) Roth, H. D. Structure and reactivity of organic radical cations. In *Photoinduced Electron Transfer IV*; Mattay, J., Ed.; Springer Berlin Heidelberg: Berlin, Heidelberg, 1992; pp 131−245.
(31) Schmittel, M.; Burghart, A. Understanding Reactivity Patterns of Radical Cations. *Angew. Chem., Int. Ed. Engl.* **1997**, *36*, 2550−2589.
(32) Odom, S. A.; Ergun, S.; Poudel, P. P.; Parkin, S. R. A fast, inexpensive method for predicting overcharge performance in lithium-ion batteries. *Energy Environ. Sci.* **2014**, *7*, 760−767.
(33) Gong, K.; Fang, Q.; Gu, S.; Li, S. F. Y.; Yan, Y. Nonaqueous redox-flow batteries: organic solvents, supporting electrolytes, and redox pairs. *Energy Environ. Sci.* **2015**, *8*, 3515−3530.
(34) Bard, A. J.; Faulkner, L. R. *Electrochemical Methods*, 2nd ed.; wiley, 2001.
(35) Narayana, K. A.; Casselman, M. D.; Elliott, C. F.; Ergun, S.; Parkin, S. R.; Risko, C.; Odom, S. A. N-Substituted Phenothiazine Derivatives: How the Stability of the Neutral and Radical Cation Forms Affects Overcharge Performance in Lithium-Ion Batteries. *ChemPhysChem* **2015**, *16*, 1179−1189.
(36) Bell, F. A.; Ledwith, A.; Sherrington, D. C. Cation-radicals: tris-(p-bromophenyl)amminium perchlorate and hexachloroantimonate. *J. Chem. Soc. C* **1969**, 2719−2720.
(37) Eberson, L.; Larsson, B.; Moberg, C.; Krautwurst, K. D.; Krogsgaard-Larsen, P.; Ryhage, R.; Isaksson, R. Electron transfer reactions in organic chemistry. IX: Acyloxylation and/or debromodimerization instead of electron transfer in the reaction between tris(4-bromophenyl) ammoniumyl and aliphatic carboxylates. *Acta Chem. Scand. Ser. B Org. Chem. Biochem.* **1986**, *40b*, 210−225.
(38) Eberson, L.; Larsson, B.; Maartmann-Moe, K.; Sæbø, J.; Fischer, G. W. Electron transfer reactions in organic chemistry. XII: Reactions of 4-substituted triarylaminium radical cations with nucleophiles; polar vs. Electron transfer pathways. *Acta Chem. Scand. Ser. B Org. Chem. Biochem.* **1987**, *41b*, 367−378.
(39) Zhao, H.; Tanjutco, C.; Thayumanavan, S. Design and synthesis of stable triarylamines for hole-transport applications. *Tetrahedron Lett.* **2001**, *42*, 4421−4424.
(40) Moshurchak, L. M.; Buhrmester, C.; Dahn, J. R. Triphenylamines as a Class of Redox Shuttle Molecules for the Overcharge Protection of Lithium-Ion Cells. *J. Electrochem. Soc.* **2008**, *155*, A129−A131.
(41) Yurchenko, O.; Freytag, D.; zur Borg, L.; Zentel, R.; Heinze, J.; Ludwigs, S. Electrochemically Induced Reversible and Irreversible Coupling of Triarylamines. *J. Phys. Chem. B* **2012**, *116*, 30−39.
(42) Ozkan, S. Z.; Bondarenko, G. N.; Orlov, A. V.; Karpacheva, G. P. Interfacial Oxidative polymerization of phenothiazine. *Polym. Sci. B* **2009**, *51*, 149−156.

https://dx.doi.org/10.1021/acs.chemmater.9b05345
Chem. Mater. 2020, 32, 3007−3017